Study of $\Sigma^{\pm}\pi^{\mp}$ production from negative kaons stopped in He^4 *

B. Riley,† I-T. Wang,‡ J. G. Fetkovich, and J. M. McKenzie§
Carnegie-Mellon University, Pittsburgh, Pennsylvania 15213
(Received 29 August 1974)

We have measured the $\Sigma^{\pm}\pi^{\mp}$ invariant mass distributions produced when K^- mesons stop in liquid He^4. The Kim and Martin-Sakitt parameterizations of the low-energy $\bar{K}N$ scattering data were used in various impulse models to calculate $\Sigma\pi$ invariant-mass distributions which were compared with the data. Neither parameterization fit the data well. Nevertheless, the evidence appears to support definite conclusions concerning the orbital atomic state from which the K^- undergoes nuclear absorption. It is found that S-state capture dominates, while there is very little D-state capture.

I. INTRODUCTION

There is a long history of attempts to understand K^-p scattering and its relationship to the properties of the $\Lambda(1405)$. The low-energy K^-p scattering data may be adequately described by either the multichannel constant K-matrix formalism first developed by Dalitz and Tuan,[1] or by the multichannel effective-range K-matrix formalism developed by Ross and Shaw.[2] Kim[3] used S, P, and D partial waves and the effective-range formalism to obtain a 44-parameter fit to the data below 550 MeV/c (incident laboratory momentum of the K^- meson). Martin and Sakitt[4] questioned the uniqueness of Kim's solution. They obtained a 9-parameter fit to the K^-p data below ~300 MeV/c using only S waves in a constant K-matrix formalism. The two fits agree reasonably well above K^-p threshold. However, they exhibit significant differences below, implying quite different values of the mass and width of the S-wave virtual bound state [usually associated with the $\Lambda(1405)$] as well as the $\bar{K}YN$ coupling constant calculated using dispersion relations.[5] More recently, additional fits to the data have been reported.[6]

Thus, the properties of the $\Lambda(1405)$ remain uncertain because of these differences in the below-threshold behavior of the $\bar{K}N$ fits. Moreover, Dalitz[7] has questioned the interpretation of the $\Lambda(1405)$ as a virtual bound state in the $\bar{K}N$ system.

In this paper we present the results of a bubble-chamber study of the reactions $K^-He^4 \to \Sigma^{\pm}\pi^{\mp}H^3$ at zero momentum. We have measured the invariant-mass distributions with about ten times the statistics of any previous experiment[8] and compared them with those predicted by an impulse model suggested by Uretsky and Bunnell.[9] The predictions of this model are found to be sensitive to the extrapolation of the K^-p amplitudes below threshold, allowing, with our data, an investigation of the validity of the existing parameterizations in otherwise inaccessible $\Sigma\pi$ mass regions. There are, however, complications which becloud the analysis. In addition to the K^-p amplitude, the impulse-model results are sensitive to the form of the nuclear wave function at large radius, as well as to the relative amounts of K^- capture from the S, P, and D orbital angular momentum states of the initial mesonic helium atom. Neither of these is well known. Therefore, in fitting our data we have varied these parameters in hopes of learning more about them.

A knowledge of the mesonic-atom orbital angular momentum states from which the K^- interact would be useful in shedding light on the K^- cascade process in He^4. This cascade process is not fully understood although the work of Fetkovich *et al.*[10] suggests that the Wightman-Condo[11] trapping mechanism accounts for the long K^- cascade time measurements[12-14] in He^4.

In Sec. II we discuss the experimental details. Section III contains a brief description of the impulse-model calculations of the $\Sigma\pi$ effective-mass distributions. In Sec. IV the details of the analysis are presented and comparisons of the data with the predictions of the model are discussed. Our conclusions are discussed in Sec. V. It is pointed out that neither the Kim nor the Martin and Sakitt parameterization describes the data well, and the implications of this result are discussed.

II. EXPERIMENTAL PROCEDURES

A. Bubble chamber

The bubble chamber used in this experiment was the 25 cm in diameter by 34 cm deep superconducting-magnet helium chamber that was built by Argonne National Laboratory and Carnegie-Mellon University. It is described in detail elsewhere.[15] Its principal feature is the high magnetic field (central value ~41 kG) which allowed pre-

cise momentum measurements. For example, 140-MeV/c pions (typical pion momentum in this experiment) with measured track lengths of 8 cm have typical momentum errors of ~2%. This was important in resolving π^+-proton mass ambiguities using rate of change of curvature. This method of mass determination was more reliable than the use of bubble density.

B. K^- beam

The chamber was exposed to the 28° K^- beam[16] at the Argonne ZGS (Zero Gradient Synchrotron). This was a two-stage separated beam approximately 24 meters long. In this exposure a transport momentum of ~650 MeV/c was used. Before entering the chamber, the beam was degraded by 9 cm of Be and 11 cm of Cu. There were 15 to 20 K^- per pulse impinging on the degrader, of which ~3 entered the chamber and ~1 stopped. There were about 10 muons in each picture, along with a large number of Compton electrons from neutron background. Scanning rules were especially designed to minimize problems caused by this background.

C. Scanning

Approximately 54 000 frames were subjected to linear scanning, in at least two of the three stereoviews, for Σ^+ and Σ^- production events. Approximately $\frac{2}{3}$ of the 54 000 frames were scanned twice. The over-all scanning efficiency was (96± 2)% for the $\Sigma^+\pi^-H^3$ events and (96 ± 1)% for the $\Sigma^+\pi^-H^3$. The Σ and its charged decay product provided the identifying signature (hereafter called a "kink"). The scanners were required to record any event with one and only one kink. Each event was recorded by making a tracing of the entire event on one view. These tracings proved to be valuable in various stages of the analysis. There were especially helpful to measurers in locating events.

Events rejected at the scanning level included the following:

(a) Those not in the defined fiducial volume.

(b) Those with more than one negatively charged outgoing track. These were mostly τ decays with a pion scatter or decay.

(c) Apparent Σ^+ events with only positively charged tracks coming from the production vertex. Such events were caused by Σ^- absorption by He^4 nuclei in which the Σ^- track (too short to have a detectable curvature) along with a track from the reaction

$$\Sigma^- + He^4 \rightarrow \Lambda + n + (pnn)$$

simulated a Σ^+ kink. [Here, (pnn) represents either bound or unbound nucleons.]

(d) Events with more than 3 tracks coming from the production vertex.

D. Measuring

Because of the intense and variable magnetic field, track reconstruction presented unique problems in this bubble chamber. All the Σ candidates were measured with a Hydel measuring machine (a film-plane-digitized coordinate recording device). In the original measurements, only the best two views—selected by the measurer—were used. A maximum of seven points, roughly evenly spaced, were measured on each long track. End points were normally measured in order that momentum from range could be determined. *Only* the end points of a track were measured if its projected length was less than 1.5 cm. One to three additional points were measured on tracks from 1.5 to 3.0 cm in length. Extreme care was exercised in measuring vertices since the Σ tracks were usually very short (~0.5 cm).

Since, in this chamber, pions were often trapped in the high field, it was necessary to require that no track be measured beyond ~100° turning angle in any view. This limit was set because TVGP (Three View Geometry Program)[17] had difficulty in reconstructing such tracks.[18] Even with this restriction, tracks having large turning angles yielded a 10% failure rate because of bad-stereo-angle failures. In all remeasurements, therefore, three views were used.

E. Event acceptance criteria

Several cuts were made on the incident K^- track to ensure that it was well measured and consistent with stopping. Based upon TVGP information, an event was rejected for any of the following reasons:

(a) K^- FRMS > 30.0,

(b) K^- length < 4.0 cm,

(c) $|K^-$ dip$| > 30°$,

(d) production vertex outside the fiducial volume,

(e) $|k_{K^-}| > 3.0$.

Here, FRMS is the root mean square deviation (in microns on the film) of measured points from the projected fitted track. The parameter k_{K^-} or "K test" in TVGP parlance provides a means to determine if a particle stopped by comparing the momentum from range and curvature for a given mass interpretation. It is defined as $k = (K_r - K_m)/\sigma_m$. The quantities K_r and K_m are, respectively, the expected curvature at the midpoint of the track as determined from its range (assuming the track stopped at its end point) and

the curvature of the TVGP fitted space curve. The fiducial volume was a cylinder with a radius of 9 cm and a length of 19 cm. The near end of the cylinder was 8 cm behind the near glass of the chamber.

Cuts (a)—(d) were imposed in order to ensure good momentum determination and thus sharper discrimination against in-flight interactions by criterion (e). If (e) was satisfied, the K^- momentum at the Σ production vertex was later set equal to zero in SQUAW (kinematic fitting program).[19] The k_{K^-} distribution should have a mean of zero and a width of 1. It is shown in Fig. 1 for the $\Sigma^-\pi^+H^3$ events. This should be compared with Fig. 2, which shows the k_{K^-} distribution for 44 τ^- decays known with high precision to have stopped.[14] The asymmetry evidenced in Figs. 1 and 2 is statistically consistent with the asymmetry of the stopped K^- used in measuring the cascade time in the same exposure.[14] This is believed to result from deficiencies in the geometry program associated with highly curving slow tracks.[18]

Some topology-dependent cuts were also imposed. Events were rejected if

(f) |dip| of any track > 80°,
(g) |dip| of Σ > 70°,
(h) π track length < 3 cm,
(i) FRMS of any outgoing track > 25,
(j) Σ length > 3.0 cm,
(k) Σ length < 0.1 cm, or
(l) prong from Σ^+ decay < 0.2 cm.

Cuts (f) through (i) were imposed to facilitate good track reconstruction. Criteria (d) and (j) were designed to eliminate bias against fast Σ's. Criterion (k) was imposed to minimize scanning biases against short Σ's. It also helped to eliminate fitting difficulties in SQUAW associated with large direction errors for short tracks. Criterion (l) was applied to eliminate scanning bias against Σ^+ events with short proton decay tracks.

F. Event identification

Events that passed the acceptance criteria were subjected to a two-step identification process. First, the k parameter for positive tracks was used to distinguish protons from π^+. This procedure separated the $\Sigma^-\pi^+$ events from the nonmesonic Σ^- events for about 98% of the Σ^- events. This technique was also about 80% efficient in distinguishing π^+ from proton decays of Σ^+. This first step in the identification process yielded a reasonably clean sample of $\Sigma\pi$ events separated into 3 groups:

(a) $\Sigma^-\pi^+$ pnn,
(b) $\Sigma^+\pi^-$ pnn, $\Sigma^+ \to p + \pi^0$,
(c) $\Sigma^+\pi^-$ pnn, $\Sigma^+ \to \pi^+ + n$.

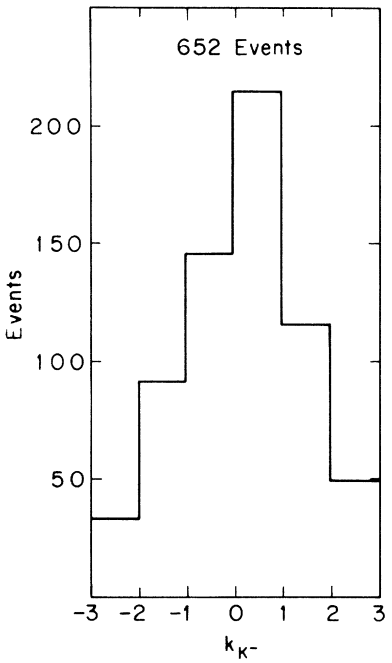

FIG. 1. k_{K^-} distribution for the final sample of K^- mesons that produced a $\Sigma^-\pi^+H^3$ final state. The corresponding distribution for K^- mesons that produced a $\Sigma^+\pi^-H^3$ final state was similar to the one shown here.

The second step consisted of hypothesis testing in the kinematics program SQUAW. However, kinematic fitting did not provide unique identification of all events. The most troublesome ambiguity arose from an inability to separate H^3 final states from "breakup" final states ("breakup" events are those with completely or partially unbound states of the pnn nucleon system). These

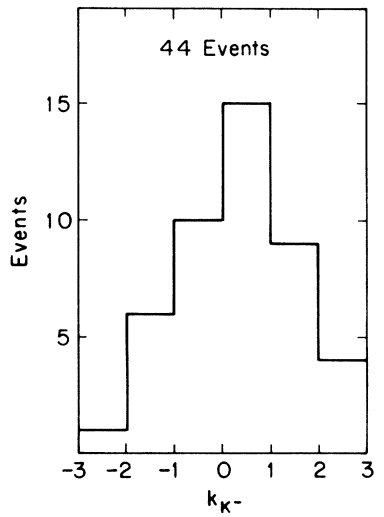

FIG. 2. k_{K^-} distribution for a sample of known stops from τ^- decays (see Ref. 14).

ambiguities exist in most of the $\Sigma\pi$ events because the breakup events were usually underconstrained. Only the $\Sigma\pi H^3$ final state is always constrained; those without a measureable H^3 prong yielded a 1C two-vertex fit, while those (approximately 20%) with a measureable H^3 prong allowed a 4C two-vertex fit (throughout the paper we use the shorthand notation "1C," for example, to mean "one constraint," etc.). Even the 4C-fit H^3 events were not uniquely identified in kinematic fitting because most of the H^3 stubs (short prongs) were less than 2 cm long, allowing a good fit (χ^2 probability > 10%) also for the dn hypothesis for ~60% of them.

A study of the distribution of the missing mass (in $K^- + He^4 \rightarrow \Sigma^-\pi^+$ mm), for events with measurable as well as those with unmeasurable H^3 stub events, led to the conclusion that those which fit the H^3 hypothesis were in fact predominately H^3 events. A scatter plot of the missing mass squared versus its error is shown in Fig. 3 for the events that fit the $\Sigma^-\pi^+H^3$ hypothesis. A similar plot for $\Sigma^-\pi^+$ events with no H^3 fit is shown in Fig. 4. The H^3 peak clearly in evidence in Fig. 3 is not seen in Fig. 4, which shows relatively more events with missing mass in the region around 2816 MeV/c^2 (mass of 3 free nucleons).

The ambiguities that existed for events which yielded both a 4C $\Sigma\pi$ H^3 fit and a 1C $\Sigma\pi$ dn fit both with χ^2 probability greater than 10% are displayed in Fig. 5. Figure 5(b) is a plot of the angle between the d and n for events that fit only the dn hypothesis (χ^2 probability > 10%). Figure 5(a) shows the same plot for the events with both H^3 and dn fits. Figure 5(b) shows isotropy, which is what one might expect for "pure" dn fits. The distribution in Fig. 5(a) is separated into two distinct regions. The region $-1.0 < \cos\theta_{nd} < 0.6$ is isotropic, while there is a forward peaking in the region $\cos\theta_{nd} > 0.6$. One would expect H^3 events that fit the dn hypothesis to exhibit such a forward peak, as was determined in a Monte Carlo simulation (see below, this section). Of course, some events in Fig. 5(a) could be $\Sigma^-\pi^+pnn$ events which fit both H^3 and dn. Also, we cannot rule out the possibility that some of the forward peak in Fig. 5(a) is due to final-state interactions

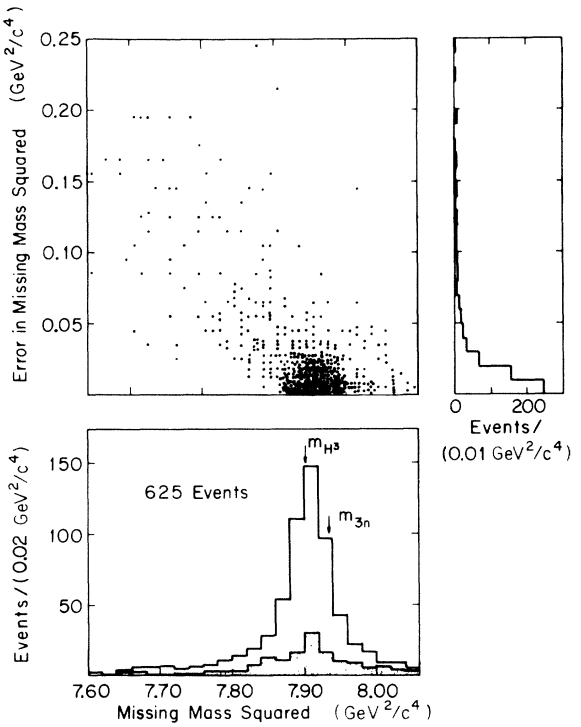

FIG. 3. Scatter plot of error in the missing mass squared ($K^- + He^4 \rightarrow \Sigma^- + \pi^+ + MM$) versus missing mass squared for the final sample of $\Sigma^-\pi^+H^3$ events. The total number of events (625) in the plot is 27 less than the total sample of 652 because measuring error causes some events to have unphysical values of Σ momentum. The shaded area in the projection of the missing mass squared are for the $\Sigma^-\pi^+H^3$ events with a 4C fit. The point labeled m_{3n} refers to the sum of rest masses of 1 proton and 2 neutrons.

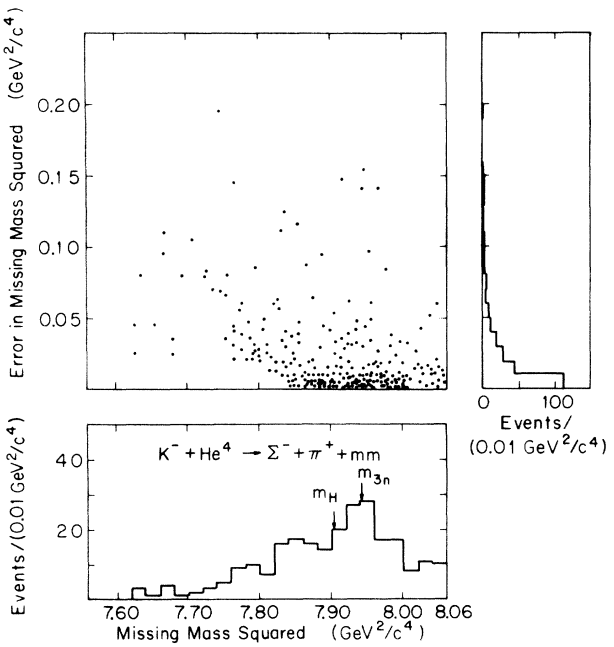

FIG. 4. Scatter plot of error of missing mass squared ($K^- + He^4 \rightarrow \Sigma^- + \pi^+ + MM$) versus missing mass squared for the $\Sigma^-\pi^+$ events that did not fit the $\Sigma^-\pi^+H^3$ hypothesis.

of the unbound dn system. However, Fig. 5 does suggest that most events ambiguous between H^3 and dn are really H^3 events.

Because of our inability clearly to extract the $\Sigma^-\pi^+pnn$ events from the $\Sigma^-\pi^+H^3$ events, we defined the final sample of $\Sigma^-\pi^+H^3$ events to be all those $\Sigma^-\pi^+$ events yielding a $\Sigma^-\pi^+H^3$ fit with a probability greater than 10%, regardless of other possible fits. The problem of statistically subtracting the background contamination is discussed below.

There is no problem in separating the pionic and nonpionic final states for the Σ^+ events. However, separation of the "breakup" from the H^3 events was complicated by the two charged decay modes of Σ^+. For example, the $\Sigma^+ \to p + \pi^0$ interpretation could lead to a $\Sigma^+\pi^- dn$ fit while the $\Sigma^+ \to \pi^+ + n$ interpretation might lead to a $\Sigma^+\pi^- H^3$ fit. In other cases, one decay interpretation would lead to a H^3 fit whereas the other would yield a fit with an unbound pnn system.

A second, well-known, difficulty with Σ^+ events arises from the fact that the $\Sigma^+ \to p + \pi^0$ decay mode yields two fits with different Σ^+ momentum values. However, only for Σ^+-p laboratory angles less than ~50° are these $p\pi^0$ ambiguities physically meaningful.

Therefore, in addition to the (χ^2 probability > 10%) acceptance criterion which was applied to the $\Sigma^-\pi^+H^3$ events, two additional criteria were applied to eliminate the $p\pi^0$ and decay mode ambiguities:

(1) The $p\pi^0$ ambiguities were separated on the basis of the lowest χ^2.

(2) The decay mode ambiguities (fit both $\Sigma^+\pi^-H^3$, $\Sigma^+ \to p + \pi^0$ and $\Sigma^+\pi^-H^3$, $\Sigma^+ \to \pi^+ + n$ with χ^2 probability > 10%) were not retained in the final sample. The Σ^+ momentum spectrum for approximately $\frac{2}{3}$ of these ambiguous events is shown in Fig. 6. Comparison with the spectrum for the final sample $\Sigma^+\pi^-H^3$ events (Fig. 7) shows them to be similar.

As a consistency check, the Σ^+ lifetime was studied as a function of the minimum accepted Σ^+ length. The results are shown in Fig. 8. A random sample of ~200 Σ^+ events yielded a lifetime of $(0.84 \pm 0.07) \times 10^{-10}$ sec (the world average is 0.80×10^{-10} sec) for a minimum length cut of 0.1 cm and a maximum length cut of 3 cm. Likewise, the Σ^- lifetime for the same length cuts was consistent with the present world average of 1.5×10^{-10} sec after a correction for a bias against long lived Σ^-. This bias was caused by Σ^- which stopped and reacted with He^4, and were therefore not picked up in the Σ scan.

As an over-all check on the data analysis, the procedures (including all decision-making computer programs) were tested using fake Monte Carlo $\Sigma^-\pi^+H^3$ events. Of the 300 generated, 129 survived all the cuts and analysis procedures.

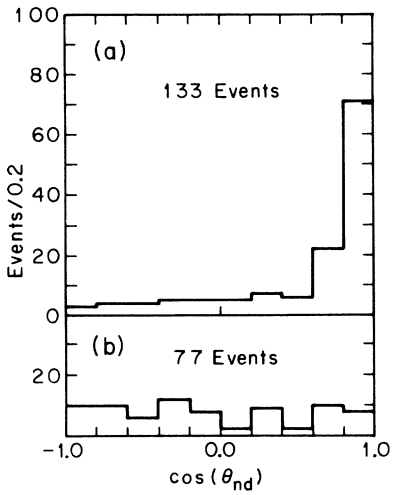

FIG. 5. (a) Distribution of the angle between the deuteron and neutron in the K^-He^4 rest frame for events that fit the $\Sigma^-\pi^+dn$ and the $\Sigma^-\pi^+H^3$ hypothesis (χ^2 probability greater than 10%). (b) Distribution of the angle between the deuteron and neutron in the K^-He^4 rest frame for events that fit the $\Sigma^-\pi\, dn$ hypothesis (χ^2 probability 10%) but that did not fit the $\Sigma^-\pi H^3$ hypothesis (χ^2 probability < 10%).

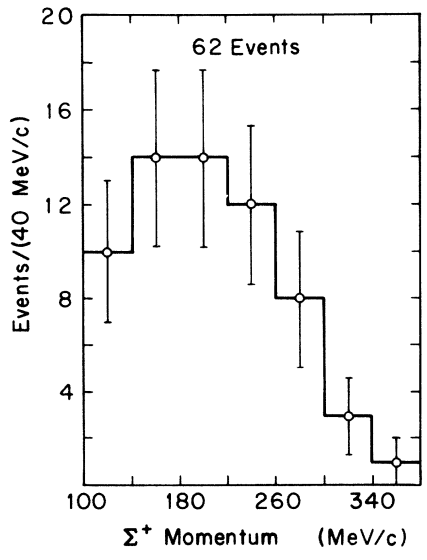

FIG. 6. Distribution of Σ^+ momentum for events with $\Sigma^+ \to p\pi^0$ and $\Sigma^+ \to \pi^+ n$ decay mode ambiguities. The histogram is for $\Sigma^+ \to p\pi^0$ mode.

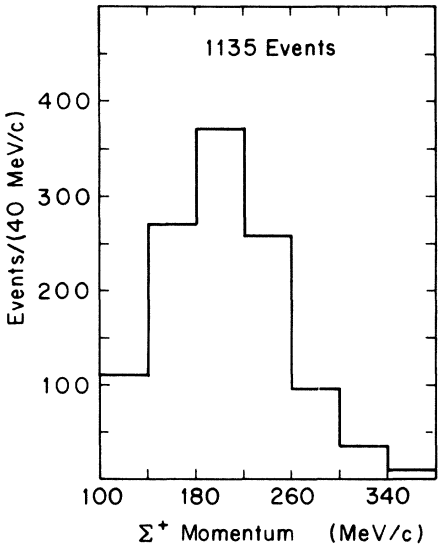

FIG. 7. Distribution of Σ^+ momentum for the final sample of $\Sigma^+\pi^-H^3$ events.

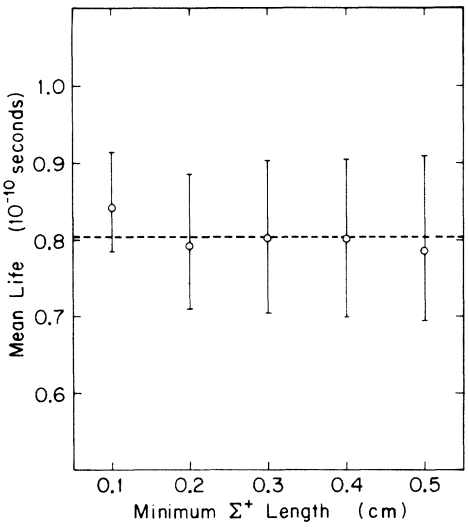

FIG. 8. Lifetime of the Σ^+ for events with a χ^2 probability greater than 10% for the $\Sigma^+\pi^-H^3$ hypothesis versus the Σ^+ minimum length cut. The final sample of $\Sigma^+\pi^-H^3$ events had a minimum length cut of 0.1 cm. The dashed line represents the world average for the Σ^+ lifetime.

Two important results emerged from these Monte Carlo studies. First, it was demonstrated that within statistics the H^3 momentum spectrum used to generate the fake events and the spectrum of those fake events surviving the analysis were identical. Secondly, about $(22\pm4)\%$ (29 of 129) of all the fake $\Sigma^-\pi^+H^3$ events fit both H^3 and the *dn* hypothesis compared to $(20\pm2)\%$ (133 of 652) of the real $\Sigma^-\pi^+$ events. Figure 9 shows the distribution of the *dn* angle for the ambiguous Monte Carlo fits. This distribution has a forward peak just as the final sample of $\Sigma^-\pi^+H^3$ events does [Fig. 5(a)], which suggests that the forward peak in the real data is due to H^3 events that fit the *dn* hypothesis.

The Monte Carlo study and the missing-mass distribution (Fig. 3) suggest that the real $\Sigma\pi H^3$ data are relatively clean except for a small number of unbound *pnn* events that cannot be eliminated on an individual basis; therefore, we have adopted the following statistical approach:

The $\Sigma\pi$ effective-mass distribution for the final sample of $\Sigma\pi H^3$ events (all events that fit the $\Sigma\pi H^3$ hypothesis with a χ^2 probability greater than 10%) was compared to various impulse model predictions using a χ^2 goodness-of-fit test. One of the parameters that was allowed to vary in finding the minimum χ^2 was the percentage of background. The shape of this background distribution was assumed to be the same as that for the "non-H^3 events" (all $\Sigma\pi$ events with a $\Sigma\pi H^3$ fit probability less than 10%). The fitting process is discussed in detail in Sec. IV.

III. THE IMPULSE APPROXIMATION

A. General considerations

The impulse approximation was first used by Fermi[20] to describe the scattering of neutrons by deuterons. The basic assumption is that the neutron interacts with only one of the nucleons in the deuteron, while the second one behaves as a spectator. This approximation applied to the present study amounts to assuming that the basic interaction is $K^- + p + (pnn)_s \rightarrow \Sigma^\pm + \pi^\mp + (pnn)_s$, where the $(pnn)_s$ is a spectator system, the components of which may or may not be bound in the final state.

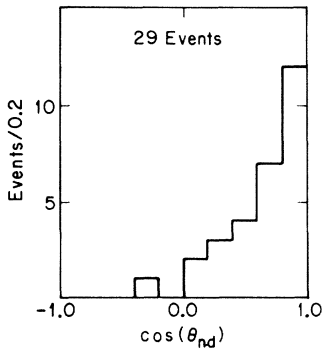

FIG. 9. Distribution of the angle between the deuteron and neutron for Monte Carlo–generated $\Sigma^-\pi^+H^3$ events which fit the $\Sigma^-\pi^+$ *dn* hypothesis with a χ^2 probability greater than 10%.

A more analytical statement of the impulse approximation[21] is given in terms of matrix elements. We define T_{fi} to be the transition amplitude $\langle \Sigma^{\pm}\pi^{\mp}H^3 | T | K^-He^4 \rangle$ and t_{fi} to be amplitude $\langle \Sigma^{\pm}\pi^{\mp} | t | K^-p \rangle$. The quantity T_{fi} is a superposition of the contributing two-body amplitudes t_{fi}. Block[22] assumed t_{fi} to be constant (i.e., momentum-independent). Uretsky and Bunnell[9] added a new feature to the model by using the Kim parameterization of the K^-p scattering data to fix the momentum dependence of t_{fi}. Since the interacting nucleon is bound, this requires the extrapolation of the $K^-p \to \Sigma\pi$ amplitudes below K^-p threshold. Kim's fit predicts a strong coupling of the $\bar{K}N$ system to the $\Lambda(1405)$, which supports the interpretation of the $\Lambda(1405)$ as a virtual bound state of the $\bar{K}N$ system. If this interpretation is correct, one might expect the $\Lambda(1405)$ to be very important in K^-He^4 interactions because the interacting proton (bound by ~20 MeV) experiences the K^-p interaction well below threshold (typically the K^-p effective mass is ~1400 MeV/c^2).

A clear test of the correctness of the $K^-p \to \Sigma\pi$ amplitudes below threshold is difficult with stopping K^- mesons because the predicted H^3 momentum spectra, or equivalently the $\Sigma\pi$ effective mass distributions (which are compared with the data), are also sensitive to the details of the form of the He^4 nuclear wave function when capture occurs from P and D orbital angular momentum states of the mesonic atom. At present, neither the atomic capture states nor the He^4 wave function at large radius are very well known. Although the simple Gaussian wave function (discussed in detail later) is generally accepted as an adequate description of the He^4 nucleus for many purposes, Dowker[23] has emphasized that it is incorrect at large radius. Furthermore, high-momentum-transfer electron scattering experiments[24] clearly indicate more structure than is reflected in a simple Gaussian wave function. Thus, in order to measure the sensitivity of our conclusions to the assumptions, we have tried several forms of the He^4 nuclear wave function and have left as free parameters to be fitted the relative amounts of S, P, and D state capture.

We refer the reader to the paper of Uretsky and Bunnell[9] for more details of the impulse model calculation and for arguments in justification of its use in this application.

B. He^4 nuclear wave functions

1. Simple Gaussian

The simplest representation of the He^4 nuclear wave function is in terms of a product of Gaussians, one factor for each pair of individual particles. One defines the spatial wave function by

$$\psi(\vec{r}_1\vec{r}_2\vec{r}_3\vec{r}_4) = N\exp\left[\frac{\lambda}{2}\sum_{i<j}^{4}(r_i - r_j)^2\right],$$

where N is a normalization constant, $\lambda = \frac{9}{32}(R_4)^2$, and R_4 is the root mean square (rms) He^4 radius.[25] We have used $R_4 = 1.44$ f, which is the charge radius obtained from electron scattering data corrected for the proton charge distribution. Only the relative coordinate r (displacement of the interacting proton relative to the center of mass of the H^3) is of importance in the present impulse calculation. In terms of this coordinate we have

$$\psi(\vec{r}) \propto \exp[-27r^2/(8R_4)^2] .$$

The rms value of r is given by $\langle r^2 \rangle^{1/2}$, where

$$\langle r^2 \rangle = \int_0^\infty r^2 |\psi(r)|^2 r^2 dr \Big/ \int_0^\infty |\psi(r)|^2 r^2 dr . \qquad (1)$$

For $R_4 = 1.44$ F the corresponding value of $\langle r^2 \rangle^{1/2}$ is 1.92 F. This value will be compared to the rms radii of other He^4 wave functions discussed below.

2. Cut-off Gaussian

One can show that the tail of the Gaussian wave function contributes very little to the rms separation of the H^3-p system. In fact, the value of $\langle r^2 \rangle^{1/2}$ is 1.90 F if the upper limit of integration in Eq. (1) above is taken to be 4 F. This value is within one standard deviation of 1.92 F. The insensitivity of the electron scattering to the assumed form of the tail of the wave function is also indicated by the fact that a modified Gaussian used by Frosch *et al.*[24] to analyze the data assumes unphysical values at $r \gtrsim 4$ F. The Frosch charge distribution is compared to the Gaussian in Fig. 10. Since the tail of the He^4 wave function is imprecisely known, we tried a "cut-off Gaussian" to compare with the simple Gaussian to test our sensitivity to the form of the tail of the wave function. It is defined by

$$\psi(r) \propto \exp[-27r^2/(8R_4)^2] \quad \text{for } r < 4 \text{ F},$$

$$\psi(r) = 0 \quad \text{for } r > 4 \text{ F}.$$

3. Exponential Gaussian

The above two wave functions fall off too rapidly at large values of r. With short-range forces, the wave function should behave exponentially in the asymptotic region. Therefore, we have also used an "exponential Gaussian" wave function:

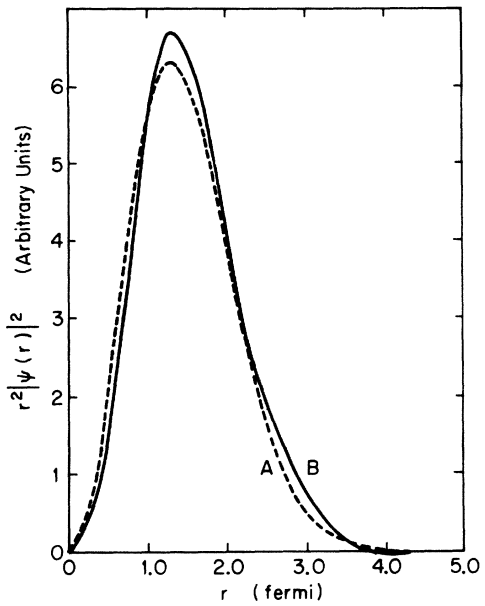

FIG. 10. Charge distribution corresponding to the modified Gaussian form of the He^4 wave function (curve B) used by Frosch *et al.* (Ref. 24) and for the simple Gaussian form of the He^4 wave function (curve A).

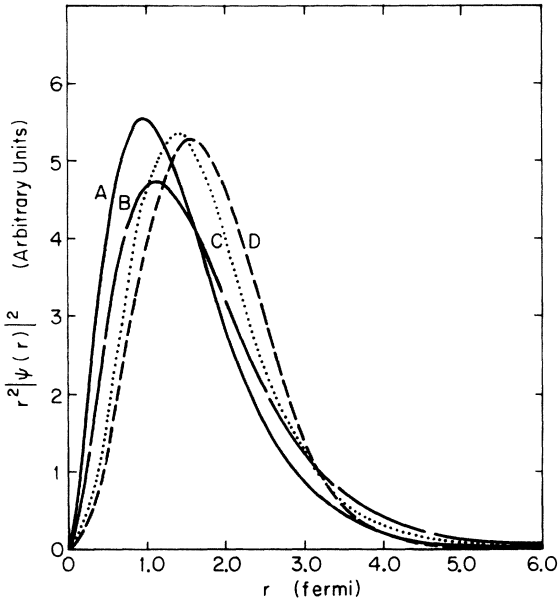

FIG. 11. Probability distribution of the H^3-proton separation r for four different forms of the He^4 wave function. Curves A, B, C, and D are for Hulthén I, Hulthén II, Woods-Saxon, and the simple Gaussian wave functions, respectively. See Sec. III of the test for the exact definitions of the wave functions.

$$\psi(r) \propto \exp[-27r^2/(8R_4)^2], \quad r < 4 \text{ F}$$

$$\psi(r) \propto N_{ex} \exp[-(MB)^{1/2}]/r, \quad r > 4 \text{ F}.$$

Here M is the reduced mass of the p-H^3 system and B is the binding energy of 19.8 MeV, giving $(MB)^{1/2}=0.85$ F. The parameter N_{ex} was adjusted to make the wave function continuous at $r=4$ F. The rms radius is 1.94 F, which is again within one standard deviation of 1.92 F, the electron scattering value.

4. *Hulthén I*

To further study the sensitivity of the model to the form of the He^4 wave function we have considered the Hulthén wave function used by Sawicki and Said[26] in their study of $\Sigma \rightarrow \Lambda$ conversion in He^4. The wave function is defined by $\psi(r) \propto (e^{-\mu r} - e^{\nu r})/r$, where r is the same p-H^3 relative coordinate as defined for the simple Gaussian. The parameters μ and ν were obtained by fitting the H^3 spectrum in the reaction $p + He^4 \rightarrow H^3 + p + p$. This method[26] yields $\mu = 0.8\ F^{-1}$ and $\nu = 1.25\ F^{-1}$ Bunnell,[27] in his study of $\Lambda\pi He^3$ production by K^- in helium, found this form to be more compatible with his data than the simple Gaussian. It is clear from Fig. 11 that the corresponding charge distribution disagrees with the Gaussian in the region $r < 4$ F. Also $\langle r^2 \rangle^{1/2}$ (separation of the H^3-p system) has a value of 1.72 F compared to the Gaussian value of 1.92 f when R_4 is fixed at 1.44 F.

5. *Hulthén II*

In order to investigate the sensitivity of the Hulthén form of the impulse model to $\langle r^2 \rangle^{1/2}$, a second set of Hulthén wave form parameters was also used. Here the parameter μ (defined above) was fixed from binding-energy considerations as for the exponential Gaussian form. Then ν was varied to give a value of 1.92 F for $\langle r^2 \rangle^{1/2}$. This method yields $\mu = 0.85\ F^{-1}$ and $\nu = 0.91\ F^{-1}$. This wave function is probably too large in the region around 4 F, where the nuclear overlap with the K^- atomic wave function seems to be important.

6. *Woods-Saxon*

The sixth form used for the He^4 wave function was a Woods-Saxon[28] type. Numerical methods were used to generate the wave function from the potential

$$V(r) = V_0/\{1 + \exp[(r-R)/a]\},$$

where $R = R_0 A^{1/3}$ F, $a = 0.65$ F, and $R_0 = 1.2$ F. The well-depth parameter V_0 was determined from the binding energy of the p-H^3 system. The parameter R_0 was arbitrarily fixed at a reasonable

value, and then a was fixed so that $\langle r^2\rangle^{1/2}=1.92$ F.

In addition to studying the effects of variation in the chosen He^4 wave function on the impulse-model predictions, we have also extended the Uretsky[9] model by substituting for the Kim parameterization[3] of the $K^-p \to Y\pi$ amplitude the Martin-Sakitt constant K-matrix parameters.[4] These were determined by fitting the K^-p scattering data below 300 MeV/c, so that only S waves were considered in the analysis. Only nine parameters are then necessary to describe the K^-p interaction. Each isospin matrix (for $I=0$ and $I=1$) is related to the K matrix by

$$I=(1-iKq)^{-1}K,$$

where q is the final relative momentum in the K^-p center-of-mass system. The Kim formalism reduces to the constant K-matrix formalism if one uses only S waves, zero effective range, and writes $K=M^{-1}$, where M is the matrix used by Kim.

As is seen below, the impulse-model results depend significantly on poorly known factors (orbital atomic state at capture and details of the nuclear wave function at large radius). For this reason an exhaustive investigation of all $\overline{K}N$ fits was not made. Rather, the Kim and Martin-Sakitt fits only were used to provide a qualitative guide to the nature and magnitude of the differences to be expected when good fits to above-threshold data are extrapolated below threshold.

IV. EXPERIMENTAL RESULTS AND ANALYSIS

In order to compare the data to the various impulse-model predictions, we fitted the measured $\Sigma\pi$ invariant-mass distributions for the $\Sigma^{\pm}\pi^{\mp}H^3$ final states to those predicted by the impulse models. The predicted distributions included effects of event losses caused by the cuts imposed on the data (see Sec. II). The agreement between various forms of the model and the data was measured by a χ^2 goodness-of-fit test. For each model chosen (i.e., each combination of He^4 wave function and t matrix), three $\Sigma\pi$ effective mass distributions were calculated: one each for assumed nuclear capture from atomic S, P, and D states. These functions were called, respectively, S, P, and D. In addition, a background distribution B was determined as described in Sec. III. The shapes of the distributions B for $\Sigma^+\pi^-$ and $\Sigma^-\pi^+$ are shown in Fig. 12. In terms of these functions we form the $\Sigma^+\pi^-$ and $\Sigma^-\pi^+$ effective-mass distribution functions, respectively, as

$$f^+=N^+(aS_+ + bP_+ + cD_+ + dB_+),$$

$$f^-=N^-(aS_- + bP_- + cD_- + dB_-),$$

where a, b, c, and d are the assumed fractions of the S, P, D, and B contributions, and N^+ and N^- are normalization constants (equal to the total numbers of events in the corresponding samples).

Finally, we form the χ^2 function

$$\chi^2=\sum_{i=1}^{k}\frac{(f_i^+-N_i^+)^2}{f_i^+ + (\sigma_i^+)^2}+\sum_{i=1}^{l}\frac{(f_i^- - N_i^-)^2}{f_i^- + (\sigma_i^-)^2},$$

where k and l are, respectively, equal to the number of data bins in the experimental $\Sigma^+\pi^-$ and $\Sigma^-\pi^+$ invariant-mass distributions. The numbers N_i^+ and N_i^- are, respectively, the numbers of Σ^+ and Σ^- events in the ith bin.

The quality $(\sigma_i^+)^2$ is added to the denominator in order to account for statistical error in the empirically determined function B. It is given by

$$\sigma_i^{+2}=\frac{(N^+)^2}{N_{B_+}}\,d^2B_{+i},$$

where N_{B_+} is the total number of events in the Σ^+ background sample. An analogous definition holds for σ_i^{-2}.

The values of a, b, c, and d were varied in minimizing χ^2 under the constraint that $a+b+c+d=1$. The results of the minimization process are summarized in Table I.

The best fits as shown in Table I have a χ^2 of ~110 for 33 degrees of freedom, which yields a confidence level of less than 0.01%. These best fits come from using the Kim rather than the

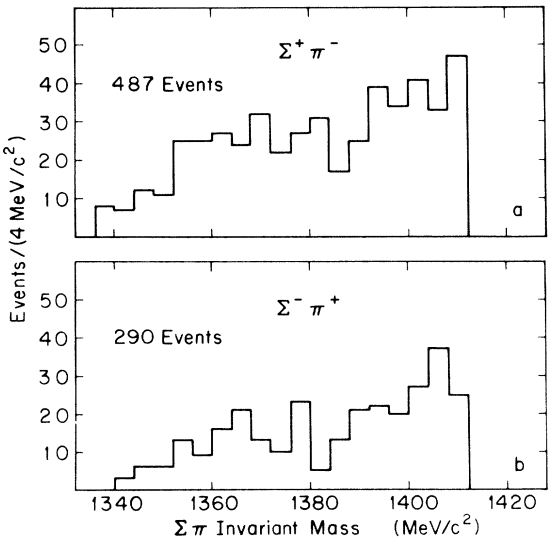

FIG. 12. Invariant mass ($\Sigma\pi$) for events that fit the (a) $\Sigma^+\pi^-H^3$ hypothesis and (b) $\Sigma^-\pi^+H^3$ hypothesis with χ^2 probability less than 10%. These distributions were used as the assumed background shapes in fitting the $\Sigma\pi H^3$ data to the impulse models.

TABLE I. The best fit χ^2 is shown for each choice of He^4 wave function, along with the fitted contributions of S, P, D orbital capture and background in the sample. The entries in the top half of the table result from use of the Kim representation for the $\bar{K}N \to \Sigma\pi$ amplitudes while those in the bottom half result from the Martin-Sakitt representation. In each case there are 33 degrees of freedom.

He^4 wave function	χ^2	Background (%)	Capture state (%) S	P	D
Gaussian (exponential)	114.2	13^{+1}_{-1}	100_{-2}	0^{+2}	0^{+1}
Gaussian (simple)	107.0	13^{+2}_{-1}	100_{-0}	0^{+0}	0^{+0}
Gaussian (cut-off)	323.3	13^{+1}_{-1}	100_{-1}	0^{+0}	0^{+0}
Hulthén I	137.8	7^{+1}_{-1}	66^{+5}_{-7}	33^{+7}_{-14}	0^{+9}
Hulthén II	106.4	10^{+2}_{-2}	58^{+5}_{-4}	42^{+5}_{-6}	0^{+3}
Woods-Saxon	317.4	6^{+1}_{-1}	100_{-1}	0^{+0}	0^{+0}
Gaussian (exponential)	182.4	17^{+1}_{-2}	48^{+5}_{-5}	52^{+6}_{-12}	0^{+10}
Gaussian (simple)	171.0	17^{+2}_{-1}	67^{+4}_{-4}	33^{+4}_{-6}	0^{+4}
Gaussian (cut-off)	173.6	17^{-2}	86^{+3}_{-3}	12^{+4}_{-5}	2^{+5}_{-2}
Hulthén I	170.6	18^{+3}_{-1}	14^{+5}_{-8}	66^{+12}_{-7}	20^{+0}_{-7}
Hulthén II	154.2	20^{+1}_{-2}	20^{+5}_{-6}	61^{+19}_{-6}	19^{+1}_{-12}
Woods-Saxon	197.2	16^{-2}	100^{+7}_{-1}	0^{+1}	0

Martin-Sakitt parameterization and imply K^- absorption mainly from the S orbital state. The $\Sigma\pi$ invariant-mass data and one of the best-fit curves for each case are shown in Figs. 13 and 14. As one might expect upon examining Figs. 13 and 14, most of the problems with the fit come from the $\Sigma^+\pi^-H^3$ final states. Our results are not sensitive to the ambiguous Σ^+ decay mode events discussed in Sec. II F. Riley[18] gives more detailed fitting results.

The sensitivity of the impulse model to the form of the t matrix, the S, P, D capture ratios, and the He^4 wave function is illustrated in Figs. 15, 16, 17, and 18. These illustrate only the $\Sigma^-\pi^+$ invariant-mass distributions, but the same behavior is observed in the $\Sigma^+\pi^-$ distributions.

The curves in Figs. 15 and 16 were generated using the Gaussian exponential wave function. The Kim fit was used to generate the curves in Fig. 15, while the Martin-Sakitt (M-S) fit yielded those in Fig. 16. One sees that the M-S fit gives curves which peak at higher $\Sigma\pi$ invariant masses than the Kim fit, resulting in a smaller apparent percentage of S-state capture (see Table I). A similar shift is observed when other He^4 wave functions are used. It appears then that the $\Sigma\pi$ mass spectrum is quite sensitive to the form of the K^-p amplitude below threshold, and hence to the mass and width of the $\Lambda(1405)$.

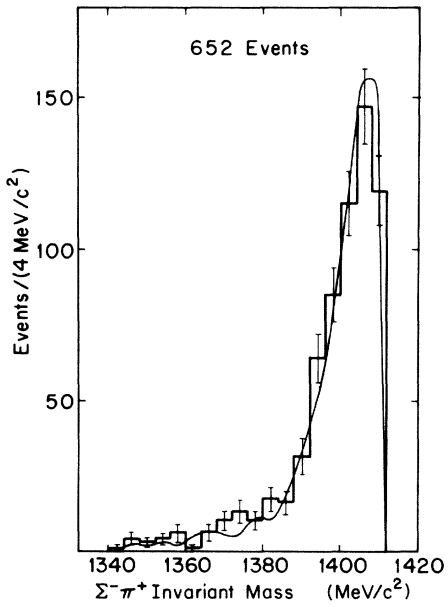

FIG. 13. $\Sigma^-\pi^+$ invariant-mass distribution for $\Sigma^-\pi^+H^3$ final states. The curve is one of the "best fits" to the data. It was generated using a simple Gaussian He^4 nuclear wave function with the Kim parameterization for the $Kp \to \Sigma\pi$ amplitude. The best-fit curve consists of 87% S capture and 13% background. See Sec. IV in the text for an explanation of the background part of the "best fit" curve.

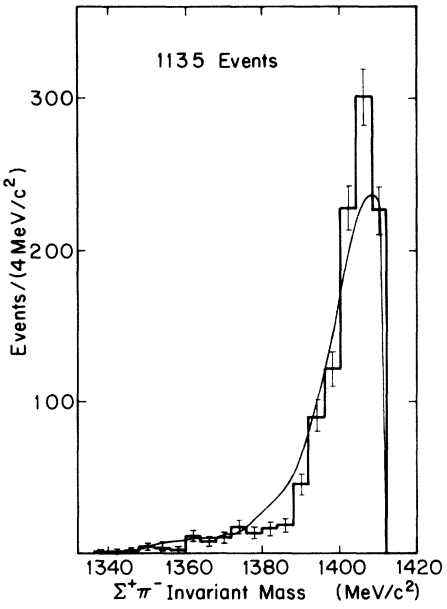

FIG. 14. $\Sigma^+\pi^-$ invariant-mass distribution for $\Sigma^+\pi^-H^3$ final states. The curve is from the same "best fit" as is shown for Σ^- in Fig. 13.

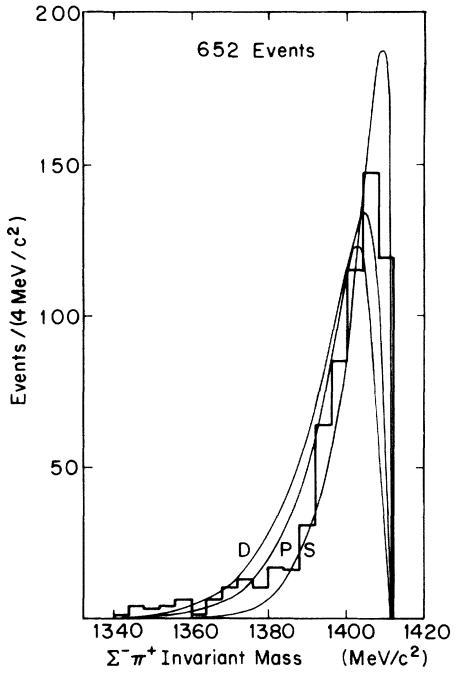

FIG. 15. $\Sigma^-\pi^+$ invariant-mass spectrum for the $\Sigma^-\pi^+H^3$ final state. The curves are the impulse-model curves generated for various He^4 wave functions and $Kp \rightarrow \Sigma\pi$ amplitude. Curve S is for pure $l=0$ orbital capture, curve P is for pure $l=1$ orbital capture, and curve D is for pure $l=2$ orbital capture. The He^4 wave function and the $K^-p \rightarrow \Sigma^-\pi^+$ amplitude used to generate the curves were, respectively, the exponential Gaussian and the Kim parameterization.

We may gain some feeling for the magnitude of the effects of variations in the He^4 wave function by comparing Figs. 15, 17, and 18, in all of which the t matrix is represented by the Kim fit, and the exponential Gaussian, cut-off Gaussian, and the Hulthén I wave function, respectively, were used to generate the mass distributions. On comparing Figs. 17 and 15, one finds that the peaks of the S, P, and D curves are shifted slightly to lower mass values. The predicted S, P, and D curves generated using the simple Gaussian peak between the curves generated using the cut-off Gaussian and those generated using the exponential Gaussian. It is clear from Figs. 15, 17, and 18 that the "pure" S capture spectrum is affected the least and the D capture spectrum shifts the most with changes in the wave function. This result is expected, since the overlap of the D orbital state of the K^- with the nuclear wave function is more dependent upon the form of the tail of the wave function than is the S-state orbital. Not only do the peaks of the S, P, and D curves shift when different wave functions are used, but they are altered appreciably at high values of $\Sigma\pi$ invariant mass. In fact, Table I shows that the Hulthén II wave function gives as good a χ^2 fit as the Gaussian exponential, but predicts only 58% S-state capture. However, the Hulthén charge distribution disagrees with electron scattering data.

Bunnell *et al.*[27] attempted to fit the He^3 spec-

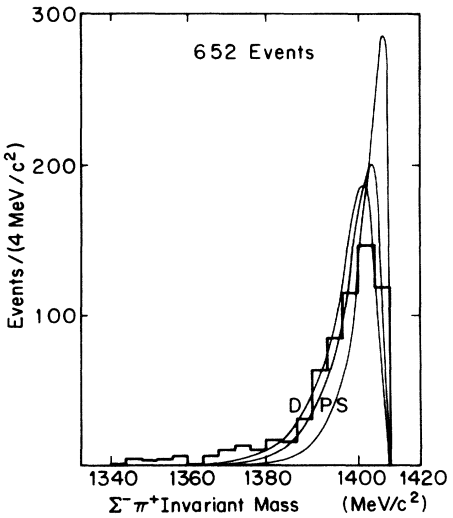

FIG. 16. The curves correspond to the exponential Gaussian wave function and the Martin-Sakitt amplitudes. The data are as in Fig. 15.

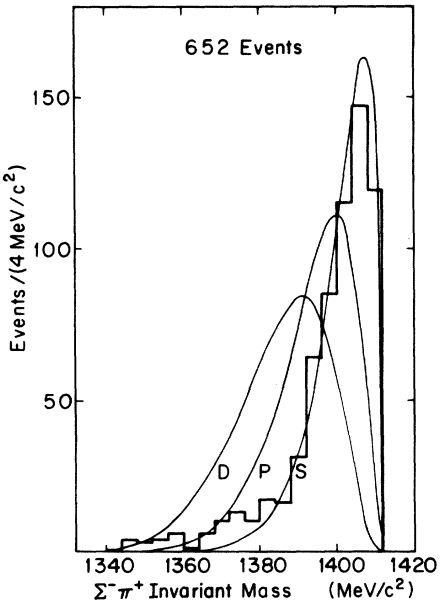

FIG. 17. The curves correspond to the cut-off Gaussian wave function and the Kim amplitudes. The data are as in Fig. 15

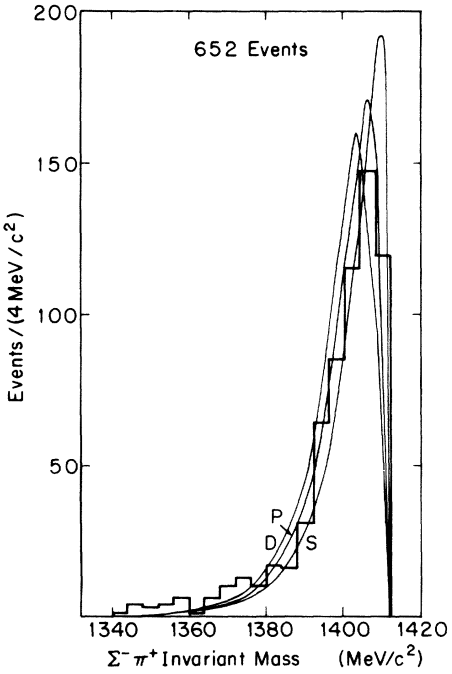

FIG. 18. The curves correspond to the Hulthén I wave function and the Kim amplitudes. The data are as in Fig. 15.

trum in the reaction $K^-He^4 \to \Lambda\pi^-He^3$ using an impulse model including the Kim parameterization with the Gaussian and Hulthén I nuclear wave functions. Their results for S- and P-state capture fractions were (they did not include the possibility of D-state capture)

Gaussian: $(60 \pm 6)\%$ S, $(40 \pm 6)\%$ P, $\chi^2 = 33$;

Hulthén I: $(15 \pm 10)\%$ S, $(85 \pm 10)\%$ P, $\chi^2 = 24$.

In both cases there were 6 degrees of freedom in the fit.

These results do not agree well with the corresponding values in Table I. Some possible causes of the disagreement are discussed in Sec. V, below. In addition, however, it should be pointed out that the two analyses are perhaps not directly comparable, because in the work of Bunnell *et al.* only a small part of the full range of He^3 kinetic energy was included, whereas here the complete H^3 spectrum was included.

V. CONCLUDING REMARKS

This experimental study of the $\Sigma\pi H^3$ final states confirms the previous result[8] that the impulse model is a good first approximation for the description of the interactions of negative kaons that are stopped in liquid helium. The "best fits" to the measured $\Sigma\pi$ invariant-mass distribution are obtained with an impulse model featuring a Gaussian or a Hulthén He^4 wave function, and the Kim $\bar{K}N$ amplitudes. The model implies predominantly S-state capture.

However, our best fits are poor and do not agree well with the results of Bunnell *et al.*[27] This may be due to any of a number of factors. The impulse model used here does not treat final-state interactions. These are known to be important, since, for example, $\Sigma \to \Lambda$ conversion occurs in He^4 with greater than 50% probability. However, another important factor may be the lack of precise knowledge of the K^-p amplitudes below threshold. Burhop[29] has suggested that the Kim and Martin-Sakitt amplitudes, below K^-p threshold, may not be adequate in heavier nuclei. Bloom *et al.*[30] have said that the $\Lambda(1405)$ must be taken into account when K^- mesons are absorbed in nuclear matter, but its properties may be different in a nucleus. Recently Chao *et al.*[31] have shown that $\bar{K}N$ scattering data above threshold is not sensitive to the parameters of the $\Lambda(1405)$. Our results indicate that in He^4, owing to the binding of the interacting nucleon, the $\Sigma\pi$ invariant-mass distribution *is* sensitive to these parameters. This is evidenced by the very different distributions generated when the Kim and the Martin-Sakitt $\bar{K}N$ amplitudes are used.

A study of $K^-He^4 \to \Sigma^{\pm}\pi^{\mp}H^3$ using slow instead of stopping K^- would be very useful in eliminating

some of the uncertainties in interpretation. The question of S, P, or D capture would not arise. Also, if the study were limited to the S-wave region, the details (e.g., in the large radius region) of the nuclear wave function would be much less important. Such work is in progress. Preliminary results suggest that $\Sigma \rightarrow \Lambda$ conversion becomes less important with in-flight K^- than with stopped K^-.

There are two inferences that may be drawn from the results (Table I), which appear not to depend significantly on the model chosen. These are that S-state capture of stopped K^- predominates, and there is little or no D-state capture. However, the reasons for the poor fits to the data must be understood before any conclusions may be stated with confidence.

ACKNOWLEDGMENTS

We thank Jack Uretsky for helpful discussions on the impulse-model calculations. We are indebted to Jack Uretsky and Kirk Bunnell for making their impulse-model program available to us, and to R. A. Sorensen and J. Johnston for providing their Woods-Saxon wave-function program. We want to express our appreciation to F. Sharkey and C. Day for their programming aid. We thank J. Rudman for his assistance in the data handling.

---

*Work supported by the U. S. Atomic Energy Commission.

†Now at the University of Evansville, Evansville, Indiana, 47702.

‡Now at Argonne National Laboratory, Argonne, Illinois, 60439.

§Now at University College, London, England.

[1]R. H. Dalitz and S. F. Tuan, Ann. Phys. (N. Y.) 10, 307 (1960).

[2]M. Ross and G. Shaw, Ann. Phys. (N. Y.) 13, 147 (1961); G. L. Shaw and M. Ross, Phys. Rev. 126, 814 (1962).

[3]J. K. Kim, Phys. Rev. Lett. 19, 1074 (1967).

[4]B. R. Martin and M. Sakitt, Phys. Rev. 183, 1345 (1969).

[5]J. K. Kim, Phys. Rev. Lett. 19, 1079 (1967).

[6]G. Ebel, A. Müllensiefen, H. Pilkuhn, F. Steiner, D. Wegener, M. Gourdin, C. Michael, J. L. Petersen, M. Roos, B. R. Martin, G. Oades, and J. J. deSwart, Nucl. Phys. B33, 317 (1971). This includes a compilation of fits to K^-p scattering data, and of coupling-constant determinations. See this article for references.

[7]R. Dalitz, invited talk at the Hyperon Resonances Conference, Duke University, 1970 (unpublished).

[8]M. M. Block, E. B. Brucker, R. Gessaroli, T. Kikuchi, A. Kovacs, C. M. Meltzer, R. Kraemer, M. Nussbaum, A. Pevsner, P. Schlein, R. Strand, H. O. Cohn, E. M. Harth, J. Leitner, L. Lendinara, L. Monari, and G. Puppi, Nuovo Cimento 20, 724 (1961); P. A. Katz, K. Bunnell, M. Derrick, T. Fields, L. G. Hyman, and G. Keyes, Phys. Rev. D 1, 1267 (1970).

[9]J. Uretsky and K. Bunnell, Phys. Rev. D 2, 119 (1970).

[10]J. G. Fetkovich, B. R. Riley, and I-T. Wang, Phys. Lett. 35B, 178 (1971).

[11]A. S. Wightman, Phys. Rev. 77, 521 (1950); G. T. Condo, Phys. Lett. 9, 65 (1964).

[12]J. G. Fetkovich and E. G. Pewitt, Phys. Rev. Lett. 11, 290 (1963).

[13]M. M. Block, J. G. Kopelman, and C. R. Sun, Phys. Rev. 140, B143 (1965).

[14]J. G. Fetkovich, J. McKenzie, B. R. Riley, I-T. Wang, K. O. Bunnell, M. Derrick, T. Fields, G. S. Keyes, and L. G. Hyman, Phys. Rev. D 2, 1803 (1970).

[15]M. Derrick, T. Fields, L. Hyman, J. Loken, K. Martin, E. G. Pewitt, J. Fetkovich, and J. McKenzie, in Proceedings of the 1966 International Conference on Instrumentation for High Energy Physics, USAEC Conference No. 660918 (unpublished).

[16]M. Derrick and G. S. Keyes, in Proceedings of the 1966 International Conference on Instrumentation for High Energy Physics (unpublished).

[17]F. T. Solmitz, A. D. Johnson, and T. B. Day, Alverez Group Programming Note No. 117, CLRL, 1965 (unpublished).

[18]B. R. Riley, Ph.D. thesis, Carnegie-Mellon Univ., 1970 (unpublished).

[19]Kinematic fitting program written by T. B. Day, O. I. Dahl, and F. T Solmitz at University of California, Lawrence Radiation Laboratory.

[20]E. Fermi, Ric. Sci. 7, 13 (1936).

[21]L. S. Rodberg and R. B. Thaler, *Introduction to Quantum Theory of Scattering* (Academic, New York, 1967), p. 341.

[22]M. M. Block, Nuovo Cimento 20, 716 (1961).

[23]J. S. Dowker, Nuovo Cimento 22, 218 (1961).

[24]R. F. Frosch, J. S. McCarthy, R. E. Rand, and M. R. Yearian, Phys. Rev. 160, 874 (1967).

[25]R. H. Dalitz and B. W. Downs, Phys. Rev. 111, 967 (1958).

[26]P. Said and J. Sawicki, Phys. Rev. 139, B991 (1965).

[27]K. Bunnell, Ph.D. thesis, Northwestern Univ., 1969 (unpublished); K. Bunnell, M. Derrick, T. Fields, L. G. Hyman, and G. Keyes, Phys. Rev. D 2, 98 (1970).

[28]R. D. Woods and D. S. Saxon, Phys. Rev. 95, 577 (1954).

[29]E. H. S. Burhop, Nucl. Phys. B44, 445 (1972).

[30]S. D. Bloom, M. H. Johnson, and E. Teller, Phys. Rev. Lett. 23, 28 (1969).

[31]Y. A. Chao, R. W. Kraemer, D. W. Thomas, and B. R. Martin, Nucl. Phys. B56, 46 (1973).

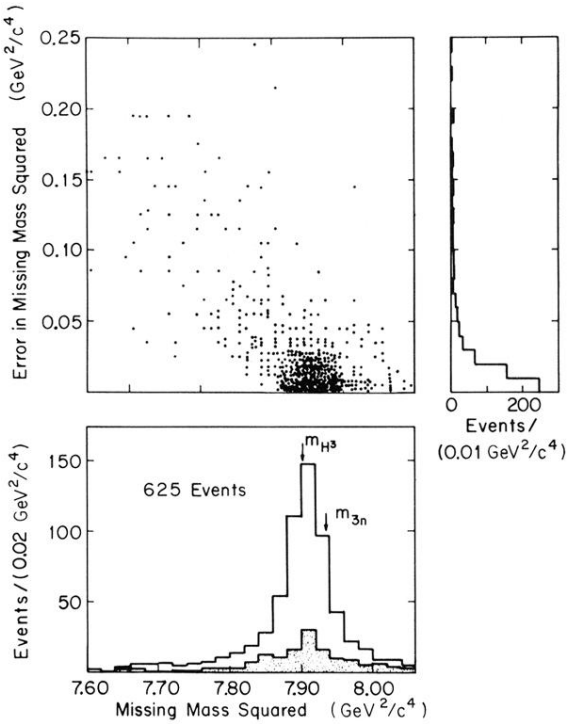

FIG. 3. Scatter plot of error in the missing mass squared ($K^- + He^4 \rightarrow \Sigma^- + \pi^+ + MM$) versus missing mass squared for the final sample of $\Sigma^-\pi^+H^3$ events. The total number of events (625) in the plot is 27 less than the total sample of 652 because measuring error causes some events to have unphysical values of Σ momentum. The shaded area in the projection of the missing mass squared are for the $\Sigma^-\pi^+H^3$ events with a 4C fit. The point labeled m_{3n} refers to the sum of rest masses of 1 proton and 2 neutrons.